Photosynthetic acclimation of *Nannochloropsis oculata* investigated by multi-wavelength chlorophyll fluorescence analysis

Milán Szabó, Kieran Parker, Supriya Guruprasad, Unnikrishnan Kuzhiumparambil, Ross McC. Lilley, Bojan Tamburic, Martin Schliep, Anthony W.D. Larkum, Ulrich Schreiber, John A. Raven, Peter J. Ralph

PII: S0960-8524(14)00890-6
DOI: http://dx.doi.org/10.1016/j.biortech.2014.06.046
Reference: BITE 13580

To appear in: *Bioresource Technology*

Received Date: 18 March 2014
Revised Date: 11 June 2014
Accepted Date: 13 June 2014

Please cite this article as: Szabó, M., Parker, K., Guruprasad, S., Kuzhiumparambil, U., Lilley, R.M., Tamburic, B., Schliep, M., Larkum, A.W.D., Schreiber, U., Raven, J.A., Ralph, P.J., Photosynthetic acclimation of *Nannochloropsis oculata* investigated by multi-wavelength chlorophyll fluorescence analysis, *Bioresource Technology* (2014), doi: http://dx.doi.org/10.1016/j.biortech.2014.06.046

Photosynthetic acclimation of *Nannochloropsis oculata* investigated by multi-wavelength chlorophyll fluorescence analysis

Milán Szabó[a,*], Kieran Parker[a], Supriya Guruprasad[a], Unnikrishnan Kuzhiumparambil[b], Ross McC. Lilley[a], Bojan Tamburic[a], Martin Schliep[a], Anthony W.D. Larkum[a], Ulrich Schreiber[c], John A. Raven[a,d], Peter J. Ralph[a]

[a]Plant Functional Biology and Climate Change Cluster, University of Technology Sydney, Broadway NSW 2007 Australia

[b]Centre for Forensic Science, University of Technology Sydney, Broadway NSW 2007 Australia

[c]Julius-von-Sachs Institut für Biowissenschaften, Universität Würzburg, Julius-von-Sachs Platz 2, 97082 Würzburg, Germany

[d]Division of Plant Sciences, University of Dundee JHI, The James Hutton Institute, Invergowrie, Dundee DD2 5DA, UK[1]

[1]Permanent address of John A. Raven

*Corresponding Author. Milán Szabó, Plant Functional Biology and Climate Change Cluster, University of Technology, Sydney, PO Box 123, Broadway NSW 2007 Australia, email: Milan.Szabo@uts.edu.au, Phone: +61-2-9514-4162

Abstract

Multi-wavelength chlorophyll fluorescence analysis was utilised to examine the photosynthetic efficiency of the biofuel-producing alga *Nannochloropsis oculata,* grown under two light regimes; low (LL) and high (HL) irradiance levels. Wavelength dependency was evident in the functional absorption cross-section of Photosystem II (σ_{II} (λ)), absolute electron transfer rates (*ETR*(II)), and non-photochemical quenching (NPQ) of chlorophyll fluorescence in both HL and LL cells. While $\sigma_{II}(\lambda)$ was not significantly different between the two growth conditions, HL cells upregulated *ETR*(II) 1.6 to 1.8-fold compared to LL cells, most significantly in the wavelength range of 440-540 nm. This indicates preferential utilisation of blue-green light, a highly relevant spectral region for visible light in algal pond conditions. Under these conditions, the HL cells accumulated saturated fatty acids, whereas polyunsaturated fatty acids were more abundant in LL cells. This knowledge is of importance for the use of *N. oculata* for fatty acid production in the biofuel industry.

Keywords: biofuels, chlorophyll fluorescence, *Nannochloropsis* spp., non-photochemical quenching, photosynthetic electron transport rate

1. Introduction

Industrial scale production of microalgae for biofuels requires that the culture conditions are maximised for both growth rate and biomass. A critical factor in optimising these two is the quantity and quality of the light incident on the culture. This imposes constraints on the configuration of outdoor ponds and enclosed photobioreactors, as well as the geographical location of the pond. Other important factors are mixing, aeration, carbon dioxide delivery and supply of nutrients. Many configurations have been tested for industrial production, the most successful and highly developed of which is the raceway-type pond (Rogers et al. in press).

Understanding the plasticity of algal physiology and photosynthetic capability under variable incident irradiances is essential to predict the utility of candidate algal species for either open (algal ponds, raceway tanks) or closed (photobioreactor) systems. Ponds are usually optimised to yield the highest level of lipid for the particular species of algae selected. Several species of microalgae are promising sources of lipids when grown for large-scale biomass and biofuel production, including the green alga *Desmodesmus* sp., the cyanobacteria *Oscillatoria* sp. and *Arthrospira* sp. grown in wastewaters (Komolafe et al., 2014), the green algae *Botryococcus* sp. and *Chlorella vulgaris* (Huang et al., 2013, 2014) and the eustigmatophycean *Nannochloropsis oculata* (Sukenik et al., 1989). The effect of various environmental factors, such as pH, concentration of carbon dioxide in the medium, and irradiance were shown to impact on lipid production of microalgae (Huang et al., 2014). Beyond these environmental parameters, the application of nanomaterials (such as CaO and MgO nanoparticles) has been found to be effective catalysts of lipid synthesis and lipid extraction procedures (Zhang et al., 2013). One of the most important environmental factors that drive primary production

via photosynthesis and fatty acid methyl ester (FAME) production is light (Sukenik et al., 1989; Pal et al., 2011), where the flux density and spectral distribution of photosynthetically active radiation are both important factors. Therefore, innovations in light delivery and subsequent capture have the potential to revolutionise the biofuel industry. Spectral modification of incident light in a photobioreactor by photoluminescent phosphors increased the rate of biomass production in *Haematococcus pluvialis* (Wondraczek et al., 2013). Genetic engineering of light harvesting antennae to enhance light absorption is a major topic in *Chlamydomonas reinhardtii* research (Ort et al., 2011). The practicability of such approaches for enhancing growth of algae for large-scale biofuel production remains to be established both technically and economically, but will require a complete understanding of the acclimation potential of the cultured alga to be able to predict the optimum spectral distribution of light energy required by the cells.

1.1 Physiology and acclimation potential of *Nannochloropsis* spp. under natural light conditions

Nannochloropsis is a member of the class Eustigmatophyceae of unicellular yellow-green coloured algae within the phylum Heterokontophyta; thus being more closely related to brown algae and diatoms than to green algae, although containing only chlorophyll (Chl) *a* as a major photosynthetic pigment and lacking the accessory chlorophyll, Chl *c*. This alga has small coccoid cells (approx. 3 µm diameter) containing one plastid (Murakami and Hashimoto, 2009). *Nannochloropsis* plays a significant role in aquaculture, where it is grown widely in outdoor ponds as a food for rotifers (Ferreira et al., 2009). The robust nature of *Nannochloropsis*, its ability to accumulate intracellular oil (Kromkamp et al., 2009), and its recently discovered suitability for

targeted genetic manipulation based on efficient homologous recombination (Kilian et al., 2011), make it a promising algal candidate for large-scale biofuel production.

For outdoor growth of microalgae in shallow ponds, the photon flux density (PFD) can vary from the midday peak of sunlight (~2,000 μmol photons.m^{-2}.s^{-1}, 400-700 nm) to relatively low light levels (~20 μmol photons.m^{-2}.s^{-1}) early and late in the day. Hence the algae must utilise PFDs ranging over two orders of magnitude. The PFD incident at the surface of such ponds is not available to all algal cells in the culture due to factors such as self-shading (where algal cells near the surface absorb light leaving lower PFDs for the cells beneath), attenuation of light by particles in the medium, as well as reflection and refraction at surfaces (Ritchie and Larkum, 2012). Under excess light conditions, photosynthetic electron transport becomes inhibited at the acceptor side of PSII as a result of limitation of reductant and ATP use by the capacity of the Calvin-Benson cycle; this restricts the electron flow from PSII. As a consequence, several photoprotective mechanisms are activated, such as compensatory increases in photosynthetic electron transport rates to acceptors other than carbon dioxide (Behrenfeld et al., 1998), adjustment of the photosynthetic light harvesting capability via effective absorption cross-section of photosynthetic reaction centres, mainly PSII (Falkowski and Kolber, 1995), and activation of excess energy dissipation mechanisms via the xanthophyll cycle, accompanied by non-photochemical quenching (NPQ) of chlorophyll fluorescence (reviewed in Raven, 2011).

The acclimation potential of *Nannochloropsis* spp. to highly variable light environments has been the subject of many laboratory studies, including recent investigations by Kromkamp et al. (2009) and Sforza et al. (2012). This alga also showed significant diurnal variation in its photosynthetic parameters under natural light

conditions, with the characteristics of sun and shade-acclimated behaviour under two essentially different photobioreactor configurations (Kromkamp et al., 2009; Sukenik et al., 2009; Tamburic et al., 2014). However, the specific impact of spectral quality of the incident light on photosynthetic reactions of *Nannochloropsis* spp. has not been investigated. The current study provides the first determination of photosynthetic parameters of *N. oculata* grown at two different irradiance levels, resolved in a wavelength-dependent manner. This information is essential for photobioreactor (PBR) applications using narrow bandwidth irradiance; the identification of regions where the spectrum of photosynthetically available radiation maximises the biomass of biofuel-producing algae.

1.2 Novel multi-wavelength chlorophyll fluorescence analysis on *Nannochloropsis* spp.

A broadly applied, non-invasive method to assess photosynthetic capability and light-acclimation state of microalgae is based on variable fluorescence of Chl *a* (e.g. Schreiber, 2004). The effective quantum yield of PSII can be readily determined at a given wavelength with pulse amplitude modulated (PAM) fluorometry (Genty et al., 1989) and based on incident photon flux density of a particular wavelength a relative rate of photosynthetic electron transport can be calculated. Problems arise when the rates of fluorescence derived electron transport which have been generated by different coloured lights are compared (Schreiber et al., 2012). In this case, the relative efficiencies with which differently coloured light is absorbed by PSII have to be taken into account. The term 'functional absorption cross-sectional area of PSII' was introduced by Ley and Mauzerall, 1982 and the method of fast-repetition rate fluorometry (FRRf) was developed to provide estimates of the optical cross-sectional

area of PSII (called σ_{PSII} in the dark- acclimated state and $\sigma_{PSII'}$ in the light-acclimated state, see e.g. Falkowski and Kolber, 1995). Based on σ_{PSII} estimates, several numerical models were developed to define absolute electron transport rates that could also provide reliable estimates of chlorophyll fluorescence-based photosynthetic productivity (Suggett et al., 2009). A spectrum of optical absorption cross-section of *Nannochloropsis* has recently been reported (Kandilian et al., 2013); this is based on the extinction coefficient of Chl *a* and, therefore, cannot be considered specific for PSII. On the other hand, chlorophyll fluorescence provides specific information on the functional wavelength-dependent absorption cross-sectional area of PSII ($\sigma_{II}(\lambda)$), which is essential for estimating overall electron transport rates from chlorophyll fluorescence parameters (Schreiber et al., 2012). With the knowledge of incident photosynthetically available radiation (PAR) and of $\sigma_{II}(\lambda)$, the actual PSII photon absorption rate, *PAR*(II), can be readily calculated. Based on *PAR*(II) and the effective PSII quantum yield determined for the same wavelength of light, Y(II), the absolute electron turnover rate of Photosystem II, *ETR*(II), an absolute, chlorophyll fluorometry-based measure of photosynthetic performance can be determined (Schreiber et al., 2012). In the current study, the acclimation potential of photosynthetic electron transport processes in *Nannochloropsis oculata* is analysed when grown at two different PFDs of white growth light, both below the usual midday peak solar irradiances, but differing 15-fold in absolute irradiance levels. As an estimate of accumulation of energy storage products, the fatty acid composition of the alga is determined under both growth conditions to better understand the potential effects of growth light intensity when *N. oculata* is utilised for biofuel production.

2. Materials and Methods

2.1 Inoculum strain and stock cultures

The microalga *Nannochloropsis oculata* (Australian National Algae Culture Collection, ANACC, strain CS-179) was grown in f/2 seawater medium, according to ANACC protocols), as suspended cultures in 250 mL Erlenmeyer flasks. These stock cultures were housed in an incubator (Labec Temperature Cycling Chamber, Labec Laboratory Equipment Pty Ltd., Australia) at 20 ˚C under fluorescent illumination (TLD 18W/54 fluorescent tubes, Philips) at PFD of 40 µmol photon.m^{-2}.s^{-1} with a 12 h/12 h light/dark cycle.

2.2 Experimental cultures

All cultures were grown as replicates (n=4) in 200 mL f/2 medium in flat-sided plastic culture vessels (19 x 11 x 3.5 cm), laid on their side and illuminated from above. The depth of the culture was 10 mm, minimising self-shading. Each flask was inoculated with 2 mL of stock culture, which was in stationary growth phase. The cultures were aerated with laboratory air using a small air pump via a stainless steel tube (outer and inner diameters of 0.95 and 0.4 mm respectively) at a rate of approximately 30 mL.min^{-1} into the culture at its centre. All cultures were grown under white LED lights (IronHorse, WLED80, Arlec, Blackburn, Australia). Two PFDs were used: low light (LL; 20 µmol photon.m^{-2}.s^{-1}) and high light (HL; 300 µmol photon.m^{-2}.s^{-1}) with a 12 h/12 h light/dark cycle provided as a square wave oscillation. The growth experiments were performed in a controlled environment room with temperature maintained at ~21 ˚C. For chlorophyll fluorescence measurements, cultures were sampled in the early exponential growth phase (four days post-inoculation), the Chl *a* concentrations were about 300 µg.L^{-1} or 0.3 µg.cm^{-2} surface area in the case of both HL

and LL cells. This was equivalent to basic Chl *a* fluorescence (F_0) values of 0.53±0.045 V with measuring light wavelength of 440 nm, intensity 1, gain 1, recorded using the Multiple Excitation Wavelength Chlorophyll Fluorescence Analyzer (MC-PAM, Heinz Walz GmbH, Germany, see below). Samples were adjusted to similar F_0 values to ensure that samples were taken at approximately the same Chl *a* content, 300 $\mu g.L^{-1}$ (determined as described below).

2.3 Determination of chlorophyll content

Chl *a* content of *Nannochloropsis oculata* cultures was determined according to the magnesium-saturated ethanol solvent procedure of (Ritchie, 2008). Cell suspensions were extracted with 100% ethanol, stored at -20 ˚C for 24 h, and centrifuged (Labogene 1580R) for 1 min at 21,000 g. The absorbance of the pigment extracts was determined at the wavelengths of 632, 649 and 665 nm using a UV-VIS spectrophotometer (Varian Cary 50 Bio, Palo Alto, CA, USA).

2.4 Multicolour PAM (Multiple Excitation Wavelength Chlorophyll Fluorescence Analyzer) measurements

2.4.1 Chlorophyll fluorescence measurement procedure

The Multiple Excitation Wavelength Chlorophyll Fluorescence Analyzer (MC-PAM; Heinz Walz GmbH, Germany) was used. Measurements were performed for each of five different colours at wavelengths of 440, 480, 540, 590 and 625 nm. Replicate samples (1.4 mL) were taken from stock cultures about four days after inoculation when the value of F_0 was ~0.53 V in the case of both HL and LL cultures (see above). Samples were placed in a quartz, 1 cm path-length cuvette, housed in the optical unit (ED-101US/MD) of the MC-PAM. Homogeneous distribution of the samples within the cuvette was maintained by a magnetic flea driven by a stirrer unit integrated into the

bottom of the optical unit. Cells were dark-acclimated for 10 min in the presence of far-red (FR) background light (setting 10). These conditions were found to be ideal to obtain the highest achievable maximal quantum efficiency of PSII ($Y(II)_{max}$) for all wavelengths of measuring light in the present study and ensured complete oxidation of the photosynthetic electron transport chain to provide consistent measurements of $Y(II)_{max}$ and $\sigma_{II}(\lambda)$ (Schreiber et al., 2012). After dark acclimation, the maximal quantum yield of PSII ($Y(II)_{max}$, corresponding to F_V/F_M in pigment state 1) was determined, using a saturating pulse (SP setting 12, width 0.6 s). For $Y(II)_{max}$ measurements, the measuring light (ML) and Gain settings were adjusted to obtain similar F_0 values for the different colours ($F_0 = 0.53 \pm 0.045$ V, n=20). After the $Y(II)_{max}$ measurement, a further 1 min dark acclimation was applied before a measurement sequence was started to determine $\sigma_{II}(\lambda)$. A pre-programmed script was used according to Schreiber and Klughammer, (2013) to determine $\sigma_{II}(\lambda)$ consecutively within one minute at all the five wavelengths. After this sequence, dark-acclimation in the presence of FR light (setting 10, see above) was re-applied for a further 5 min to return the photosynthetic electron transport chain to the reference re-oxidised state. An automated steady-state light curve (SSLC) measurement was then performed at each wavelength to determine the relative electron transport rates (rETR, see below). From these and the $\sigma_{II}(\lambda)$ values, the absolute rates of PSII turnover ($ETR(II)$) were calculated.

2.4.2 Determination of the PFD for each wavelength (establishing the PAR list)

The US-SQS/WB Spherical Micro Quantum Sensor (Heinz-Walz GmbH, Germany) was placed centrally in the quartz cuvette containing f/2 medium. The quantum sensor was directly connected to the MCP-C Control Unit of the MC-PAM and an automated routine by the PamWin-3 software was used to obtain the "PAR lists" for all

wavelengths, which was saved and used for all measurements performed in the current communication. Based on these lists the PamWin-3 user software of the instrument automatically calculates the PFD values for all settings and wavelengths of pulse-modulated measuring light, continuous AL and multiple turnover pulses.

2.4.3 Optimisation procedure for measurements of $\sigma_{II}(\lambda)$

In order to determine the absorption cross-sectional area of PSII, consecutive measurements of the O-I_1 fluorescence rise kinetics were performed for each wavelength under reference conditions. A pre-programmed fast kinetic trigger file (Sigma1000.FTM) was used including triggering of a saturating single turnover pulse (ST, duration of 50 µs) at the end of a 1 ms illumination period with strong actinic light (AL) of various colours (Schreiber et al., 2012). Minimal fluorescence yield (designated as 'O' in the fast fluorescence terminology) with all PSII reaction centres open was measured during a 100 µs period preceding onset of actinic illumination. Sufficiently high light intensities were used to assure substantial closure of PSII reaction centres during the standard 1 ms long actinic illumination period. The saturating multi-colour ST at the end of this period served for full closure of PSII and determination of the corresponding fluorescence level (I_1-level). Consecutive O-I_1 rise kinetics was recorded for each wavelength using special script files. ML intensity and gain were adjusted to obtain similar F_0 values and the AL intensities were adjusted to obtain similar initial rise kinetics for all wavelength.

2.4.4 Steady-state light curve (SSLC)

SSLCs were recorded according to Schreiber et al. (2012). Light response curves of relative ETR (rETR) were recorded using the Light Curve Program files in PamWin-3. In general, the same wavelength was used for ML and AL. Step width at each intensity

setting was 3 min. The low-intensity steps were covered by ML at high settings of pulse frequency. New cell suspensions were used for each new set of measurements after a different matching wavelength of ML and AL was applied.

2.5 Calculation of photosynthetic electron transport rates

Relative electron transport rates were calculated as

$$\mathrm{rETR} = \mathrm{Y(II)} * \mathrm{PAR} * \mathrm{ETR\ factor} \quad (1)$$

where rETR is the relative electron transport rate, Y(II) is the effective quantum yield (defined as $Y(II)_{max}$ in the dark-adapted state as maximal quantum efficiency of PSII), PAR is the incident irradiance based on the PAR list of the instrument (in µmol photons. m^{-2}. s^{-1}) and ETR factor is the fraction of light absorbed by the sample and distributed to PSII (for rETR calculations, ETR factor of 0.42 was used arbitrarily, since true PSII absorption requires quantitative information on the PSII absorption cross-section).

The photon absorption rate (PAR(II)) was calculated as

$$PAR(\mathrm{II}) = \sigma_{\mathrm{II}}(\lambda) * \mathrm{L} * \mathrm{PAR} \quad (2)$$

Where PAR(II) is the photon absorption rate (in photons.$PSII^{-1}$.s^{-1}), $\sigma_{II}(\lambda)$ is the absorption cross-sectional area of PSII (in nm^2), L is Avogadro`s constant and PAR is the incident irradiance based on the PAR list of the instrument (in µmol photons.m^{-2}.s^{-1}).

The electron turnover rate of PSII (ETR(II), expressed as electrons.$PSII^{-1}$.s^{-1}) is calculated as:

$$ETR(II) = PAR(II) * [Y(II)/Y(II)_{max}] \quad (3)$$

where Y(II) is the effective quantum yield and $Y(II)_{max}$ is the maximal quantum efficiency of PSII.

2.6 Fatty acid extraction and analysis

N. oculata cells (200 mL) were harvested from flat-sided plastic culture flasks (n=3) by centrifugation at 3600 g for 10 minutes. Cells were washed by three repeated cycles of centrifugation and re-suspension in the same volume of 0.1 M phosphate buffer, followed by freeze drying. Lyophilized biomass was weighed to calculate the amount of biomass for each treatment. Direct transesterification of biomass containing a known amount of heptadecanoic acid (internal standard; Sigma Aldrich, NSW, Australia) using methanol:chloroform:hydrochloric acid mixture (10:1:1 v/v) was carried out as described in Dunstan et al. (2007). Following transesterification, the upper organic layer containing fatty acid methyl esters (FAME) was extracted and evaporated to dryness under nitrogen. The residue was used to calculate total FAME per g biomass and further reconstituted in 200 µL of hexane and was analysed using an GC-MS (Agilent 7890 series GC coupled to an Agilent quadrupole MS (5975N)) on a HP-5MS fused silica capillary column (5%-phenyl-methylpolysiloxane, 30 m long, 0.25 mm i.d., film thickness 0.25 µm, Agilent Technologies). Samples were injected in splitless mode at an inlet temperature of 280 ˚C. The GC temperature programming rates were followed according to Dunstan et al. (2007). Peaks were identified using high purity fatty acid (99.9%) standards (Sigma Aldrich, NSW, Australia) and quantified using software (Agilent Mass Hunter).

3. Results and Discussion

3.1 Wavelength-dependent absorption cross-sectional area of PSII in *N. oculata*

The wavelength-dependent absorption cross-sectional area of PSII ($\sigma_{II}(\lambda)$) values (Fig. 1) were maximal at 440 nm (mostly related to the blue absorption band of Chl *a*, but also to carotenoids) and decreased towards minimal values at 540 nm. From 540 nm they increased progressively towards 625 nm. Compared with the $\sigma_{II}(\lambda)$ spectrum of the green alga *Chlorella sp.* (Schreiber et al., 2012), that of *N. oculata* shows some differences, especially the much smaller value at 480 nm. This is a consequence of the absence of accessory chlorophylls, such as Chl *c* in *N. oculata*, which typically absorb at 460-480 nm when present. $\sigma_{II}(480)$ is determined mainly by the xanthophylls violaxanthin and vaucheriaxanthin, that act as light-harvesters in *N. oculata* (Whittle and Casselton, 1975; Chrystal and Larkum, 1986). The spectra of $\sigma_{II}(\lambda)$ were essentially identical for LL and HL-grown *N. oculata*, apart from the apparent slightly higher value for $\sigma_{II}(440)$ in HL cells. This suggests that acclimation to different PAR during growth does not involve adjustments in the cross-sectional area of PSII of *N. oculata* between 480 and 625 nm. These findings for $\sigma_{II}(\lambda)$ are in agreement with a recent study showing that the optical cross-sectional area of *N. oculata* is largely independent of the incident irradiance during growth (Kandilian et al., 2013), performed under optical conditions similar to those applied in the current study. However, this cross-sectional area was normalised to total Chl *a* content, and therefore cannot be interpreted as an intrinsic property of the photon absorption into PSII. Here, the O-I_1 kinetics-based derivation of cross-sectional area of PSII has the great advantage of being independent of Chl *a* content (in optically thin suspensions); moreover, no substantial differences in Chl *a* content or F_0 values between HL and LL cells were observed. Thus, $\sigma_{II}(\lambda)$ can be

considered an intrinsic property of PSII units with their sample-specific antenna system rather than an optical cross-section of Chl *a* molecules, and changes in $\sigma_{II}(\lambda)$ do not play a role in the adjustment of light-harvesting capability in *N. oculata* cells during light intensity acclimation. In this context, it has to be considered that $\sigma_{II}(\lambda)$ is defined for a quasi-dark adapted reference state and that any short-term adaptive changes occurring during illumination will be reflected in the ratio of effective to maximal PSII quantum yield, $Y(II)/Y(II)_{max}$ (Schreiber et al., 2012).

3.2 Photochemical efficiency and photoprotective capability of *N. oculata* assessed at different wavelengths

In order to characterise the quantum efficiency of photosystem II and the photoprotective capability of *Nannochloropsis oculata* grown under different light regimes, steady-state light curve measurements of the fluorescence parameters Y(II) and NPQ using MC-PAM with the same optical configuration and at the same wavelengths used for $\sigma_{II}(\lambda)$ measurements were recorded (Fig. 2).

The effective quantum yield of PSII (Y(II)) declined as a function of irradiance, when measured at 440 (Fig. 2a) and at 540 nm (Fig. 2b), at which wavelengths the maximal and minimal σ_{II} was observed, respectively. At both wavelengths, the Y(II) of LL cells declined more rapidly than HL, due to the fact that LL cells were acclimated to 15-fold lower PFD (20 µmol photon.m^{-2}.s^{-1}) than HL cells (300 µmol photon.m^{-2}.s^{-1}). Both HL and LL cells became saturated at much higher PAR when 540 nm light was used as compared to 440 nm excitation light, which is in agreement with the fact that 440 nm light is the most absorbed, whereas 540 nm is the least absorbed PSII light (according to $\sigma_{II}(\lambda)$, Fig. 1). Non-photochemical quenching (NPQ) parameters,

calculated from the same light curves as the Y(II) plots are also shown in Fig. 2. Distinctly higher NPQ values were induced by the 440 nm light (Fig. 2c) than the 540 nm light (Fig. 2d), for both HL and LL cells. Although the induction of NPQ occurred at somewhat higher PAR values of 440 nm AL in HL cells than in LL cells, the maximum NPQ differed only minimally between the two cell types. For 540 nm light, a much higher PAR was necessary to induce any NPQ, especially in HL cells.

In order to compare parameters Y(II) and NPQ at all wavelengths available with the MC-PAM, these parameters are plotted at two irradiance levels (300 and 1200 µmol photons.m^{-2}.s^{-1}) , i.e. at sub-saturating and saturating irradiances as a function of wavelength (Fig. 3). In the case of Y(II) plots (Fig. 3a), the values recorded at the beginning of the SSLC measurements (in dark-adapted state, $Y(II)_{max}$) are also shown. Values of $Y(II)_{max}$ approaching 0.7 at all wavelengths would indicate that maximal quantum efficiency of PSII was obtained for all wavelengths in the dark-adapted state; the same reference state that was applied for the $\sigma_{II}(\lambda)$ measurements. Both in LL and HL cells, the highest values of Y(II) during steady-state illumination could be observed at 540 nm, with progressively lower values at 590 and 625 nm, and a more pronounced decline as wavelength decreased at 480 and 440 nm. While this tendency was already apparent with moderate AL (300 µmol photons.m^{-2}.s^{-1}), the largest differences were observed with high AL (1200 µmol photons.m^{-2}.s^{-1}), applied towards the end of SSLC measurement. The smaller decline of Y(II) in the case of HL cells indicates their greater electron transport capacity acquired during growth at high irradiance. The plot of NPQ as a function of wavelength (Fig. 3b) reveals that at moderate AL (300 µmol photons.m^{-2}.s^{-1}), substantial NPQ was induced only by blue AL (440 nm) with HL cells and by 440 and 480 nm light with LL cells. At high AL irradiance levels, large NPQ

values were induced in both LL and HL cells by 440 and 480 nm light, and distinctly lower values at 590 and 625 nm, with NPQ minima at 540 nm, in accordance with the $\sigma_{II}(\lambda)$ spectrum shown in Fig. 1.

Earlier studies suggested that *Nannochloropsis* spp. exhibits limited capacity for NPQ, indicating that this microalga does not utilise NPQ as a major photoprotective mechanism (Kotabova et al., 2011). However, the multi-wavelength approach shows clearly that *N. oculata* can exhibit large NPQ values that are distinctly greater with 440 nm than with 625 nm light, which can be readily explained by the fact that PSII absorption at 625 nm is only about a quarter of that at 440 nm (Fig. 1). Therefore, when blue light is used as an actinic source, NPQ is activated at much lower PAR and can reach a value of 3.5 to 4, indicating that the blue-green region of the PAR does induce efficient photoprotective mechanisms in *Nannochloropsis oculata.*

3.3 Relative electron transport rates (rETR) of *N. oculata*

The relative rate of photosynthetic electron transport (rETR) is useful for characterising the light-acclimation state of photosynthetic organisms and for providing estimates of photosynthetic efficiency and capacity, which can be done with standard equipment even under field conditions. Provided that the same organism is investigated using the same wavelength of light under different physiological states, there is no need to quantify ETR in absolute units. However, large differences in rETR light response curves have to be expected when the responses to differently coloured light are compared (Schreiber et al., 2012).

The maximal electron transport rates ($rETR_{max}$) and the light intensities at which the saturation of the SSLC occur (E_k) are shown in Figures 4a and 4b, respectively. The

spectra of both $rETR_{max}$ (Fig. 4c) and E_k (Fig. 4d) are the inverse of the spectrum of $\sigma_{II}(\lambda)$, meaning that the saturation and maximal rates of electron transport rates are minimal at 440 nm (where the absorption cross-section is the highest) and maximal at 540 nm (where the absorption cross-section is the lowest). Cells grown at HL show an approximately 1.6-fold higher $rETR_{max}$ and E_k value, indicating the different light acclimation status to LL cells. It has to be noted however, that rETR parameters at a given wavelength cannot be used as true values for electron turnover rates of PSII, unless the cross-sectional area of PSII determined at the same wavelength (fulfilled in this study), and the photon absorption rate of PSII (*PAR*(II)) is calculated (see below). Since there are minor differences in $\sigma_{II}(\lambda)$ between HL and LL treatments, *PAR*(II) was calculated to enable a better comparison between absolute electron transport rates of PSII. The relative and absolute electron transfer rates are compared in Fig. 5 at the two wavelengths, 440 and 540 nm, absorbed to a maximal and minimal extent, respectively. It is apparent that the large differences in the light response curves of rETR with 440 and 540 nm illumination (Fig. 5, panels a and b) almost disappeared when *ETR*(II) is plotted vs. *PAR*(II). On one hand, this finding suggests that the overall rate of photosynthetic electron transport in *N. oculata* is determined by *PAR*(II), independently of the wavelength. The deviations between the 540 and 440 nm *ETR*(II) light response curves at high light intensities (above 300 μmol photons.m^{-2}.s^{-1}) could be due to differences in PSI excitation. Equal rates of quantum absorption by PSII are not necessarily paralleled by equal rates of quantum absorption by PSI. Differences may become apparent when excess light can be utilized by PSI for e.g. cyclic electron transport. However, other explanations may apply (see below).

3.4 Wavelength-dependent electron turnover rates of photosystem II in *N. oculata*

Identical PAR values of the irradiance applied during the course of a light response curve may correspond to widely different rates of quantum absorption by PSII, depending on the wavelength of light. At the same PAR, PSII absorption of 440 nm light is about seven times higher than of 540 nm light, as reflected by the $\sigma_{II}(\lambda)$ values (Fig. 1). When $\sigma_{II}(\lambda)$ values are known, PAR values can be readily transformed into *PAR*(II) values, ie. the rate of quantum absorption by PSII (in units of photons.$PSII^{-1}.s^{-1}$), forming the basis for the calculation of absolute electron transfer rates (*ETR*(II)) (Fig. 5). *ETR*(II) curves can be fitted similarly to rETR curves, and the maximal electron transfer rates ($ETR(II)_{max}$) can be calculated (Fig. 6a).

The $ETR(II)_{max}$ values of LL cells were between 160 and 200 electrons.$PSII^{-1}.s^{-1}$. This means that *N. oculata* cells, growing near their limit of quantum requirement for photosynthesis are still capable of displaying relatively high electron turnover rates that are similar to those of *Chlorella* sp. (Schreiber et al., 2012), indicating efficient light utilisation at rather low growth irradiance levels. Most importantly, HL cells increased their $ETR(II)_{max}$ by about 1.4-1.8 times, exhibiting a pronounced wavelength dependency. To compare the changes in electron transport rates between HL and LL cells, the ratio of the *ETR*(II) in HL and LL cells is plotted in Fig. 6b.

While on average, the electron transport rate was ~1.6-fold higher in HL-grown than in LL-grown *N. oculata*, there was a clear trend for the HL/LL *ETR*(II) ratio to decrease from about 1.8 at 440 nm to about 1.4 at 625 nm. This suggests that acclimation of the cells to HL conditions not only enhancing electron transport efficiency, but also some specific changes such as enhancing the efficiency of light in the blue-green region of the spectrum. As the observation was already pointed out in the discussion of the data in

Fig.5, the large differences between 540 and 440 nm light curves of rETR mostly disappear, when *ETR*(II) is plotted vs. *PAR*(II). As apparent from Fig. 6a; however, substantial differences remain particularly in the case for HL cells, when $ETR(II)_{max}(440)$ is compared with $ETR(II)_{max}(625)$. This observation is closely linked with the notion that HL conditions are particularly effective in enhancing the capacity of overall electron transport upon illumination with blue light. While the mechanistic details of such enhancement are not known and have to be clarified by future work, it may be speculated that HL conditions change the PSII/PSI ratio and that 440 nm photons may be more strongly absorbed in PSI than photons at other wavelengths. It should be noted that HL refers to a high intensity of white LED light, the spectrum of which displays a pronounced peak at around 450 nm. Hence two types of "acclimation pressure" on the organism should be considered, the first being electron pressure (caused by limiting dark reactions) and the second, photoinhibition (caused by excess light), with the second being enhanced by the first. From the data presented in the current study, the extent of photoinhibition using the various wavelengths of PAR cannot be estimated. Recently an action spectrum of photoinhibition was determined for *Chlorella* using the MC-PAM (Schreiber and Klughammer, 2013), which differs substantially from a σ_{II} spectrum (i.e. PSII action spectrum) by additional action in the blue spectral region. If, as suggested in this previous study, this additional action reflects direct photodamage of the Mn-cluster of the oxygen evolving complex (Hakala et al., 2005), this damage may be unavoidable, but may be compensated by efficient repair. A complete action spectrum of *N. oculata* across all PAR wavelengths is therefore required. Further experiments will be necessary to determine the extent of net photoinhibition at various wavelengths in *N. oculata*. It is proposed that relatively

higher values of *ETR*(II) of HL cells in the blue spectral region is linked with a photo-acclimative change in response to increased irradiance in the blue region.

3.5 Fatty acid methyl ester (FAME) composition of *N. oculata*

The FAME composition of *N. oculata* grown under the two different light regimes is presented in Table 1. The major fatty acids were 16:0, 16:1 n-7, 18:1 n-9 and 20:5 n-3 with minor presence of 18:0, 18:2 n-6, 18:3 n-6, 18:2 n-3 and 20:4 n-6, in agreement with previous findings (Sukenik et al., 1989). The proportions of saturated fatty acids were slightly higher in HL cells, as was the proportion of 16:0, 18:0, 16:1 and 18:1 FAMEs. The percentage of 20:5 n-3 FAME was substantially lower in HL cells. These results indicate that *N. oculata* cells, exhibiting relatively higher absolute electron transport rates (HL conditions, Fig. 6a), are optimal sources of saturated fatty acids whereas, under LL conditions, PUFA production is higher. FAME content of HL and LL cells were similar (Table 1). The total amount of FAMEs compares with the total lipid content of 7.9 g.100 g^{-1} dry weight measured on *N. oculata* cells grown at 20 ˚C and 70 µmol photons.m^{-2}.s^{-1} (Converti et al., 2009), probably indicating that lipid classes other than fatty acids were present. Nevertheless, the two light regimes clearly affected the FAME composition of the cells.

Conclusion

The productivity of *N. oculata* and other algal species is ultimately determined by the effectiveness of their photosynthesis. This study presents new insights into the photosynthetic capabilities and lipid production of microalgae that experience order of magnitude differences in growth irradiance, both as light absorption and quantitative measure of photosynthetic electron transport rate. Elevated growth irradiance was found

to be ideal for both enhanced photosynthetic activity and production of saturated fatty acids, preferred for biofuel production. Additionally, *Nannochloropsis oculata* has the potential to selectively acclimate to distinct spectral regions of photosynthetically available radiation, with strong preference to blue-green light.

Supplementary material

The experimental setup and the spectrum of the LED source that was used for the experiments (Section 2.2) are depicted in Supplementary material.

Acknowledgements

The University of Dundee is a registered Scottish charity, no SC 015096. The authors thank David Bishop and Ronald Shimmon for their timely help and technical support.

References

[1] Behrenfeld, M.J., Prasil, O., Kolber, Z.S., Babin, M., Falkowski, P.G. 1998. Compensatory changes in Photosystem II electron turnover rates protect photosynthesis from photoinhibition. Photosynth. Res. **58**(3), 259-268.

[2] Chrystal, J., Larkum, A.W.D. 1986. Pigment-protein complexes and light harvesting in eustigmatophyte algae, in: Biggins J. (Ed.), Progress in Photosynthesis Research. Martinus Nijhoff, Dordrecht, pp. 189-193.

[3] Converti, A., Casazza, A.A., Ortiz, E.Y., Perego, P., Del Borghi, M., 2009. Effect of temperature and nitrogen concentration on the growth and lipid content of *Nannochloropsis oculata* and *Chlorella vulgaris* for biodiesel production. Chem. Eng. Process.: Process Intensif. **48**(6), 1146-1151.

[4] Dunstan, G.A., Elliott, N.G., Appleyard, S.A., Holmes, B.H., Conod, N., Grubert, M.A., Cozens, M.A. 2007. Culture of triploid greenlip abalone (Haliotis

laevigata Donovan) to market size: Commercial implications. Aquaculture. **271**, 130–141.

[5] Eilers, P.H.C., Peeters, J.C.H. 1988. A Model for the relationship between light-intensity and the rate of photosynthesis in phytoplankton. Ecol. Model. **42**(3-4), 199-215.

[6] Falkowski, P.G., Kolber, Z. 1995. Variations in chlorophyll fluorescence yields in phytoplankton in the world oceans. Aust. J. Plant Physiol. **22**(2), 341-355.

[7] Ferreira, M., Coutinho, P., Seixas, P., Fabregas, J., Otero, A. 2009. Enriching Rotifers with "Premium" Microalgae. Nannochloropsis gaditana. Mar. Biotechnol. **11**(5), 585-595.

[8] Genty, B., Briantais, J.M., Baker, N.R. 1989. The relationship between the quantum yield of phyotosynthetic electron-transport and quenching of chlorophyll fluorescence. Biochim. Biophys. Acta **990**(1), 87-92.

[9] Hakala, M., Tuominen, I., Keranen, M., Tyystjarvi, T., Tyystjarvi, E. 2005. Evidence for the role of the oxygen-evolving manganese complex in photoinhibition of Photosystem II. Biochim. Biophys. Acta-Bioenerg. **1706**(1-2), 68-80.

[10] Huang, Y.T., Lee, H.T., & Lai, C.W. 2013. Engineering of the growth environment of microalgae with high biomass and lipid productivity. J. Nanosci. Nanotechnol. **13**(3), 2117-2121.

[11] Huang, Y.T., Su, C.P. 2014. High lipid content and productivity of microalgae cultivating under elevated carbon dioxide. Int. J. Environ. Sci. Technol. **11**(3), 703-710.

[12] Kandilian, R., Lee, E., Pilon, L. 2013. Radiation and optical properties of Nannochloropsis oculata grown under different irradiances and spectra. Bioresour. Technol. **137**, 63-73.

[13] Kilian, O., Benemann, C.S.E., Niyogi, K.K., Vick, B. 2011. High-efficiency homologous recombination in the oil-producing alga Nannochloropsis sp. Proc. Natl. Acad. Sci. **108**(52), 21265-21269.

[14] Komolafe, O., Velasquez Orta, S.B., Monje-Ramirez, I., Noguez, I.Y., Harvey, A.P., Orta Ledesma, M.T. 2014. Biodiesel production from indigenous microalgae grown in wastewater. Bioresour. Technol. **154**, 297-304.

[15] Kotabova, E., Kana, R., Jaresova, J., Prasil, O. 2011. Non-photochemical fluorescence quenching in Chromera velia is enabled by fast violaxanthin de-epoxidation. Febs Lett. **585**(12), 1941-1945.

[16] Kromkamp, J.C., Beardall, J., Sukenik, A., Kopecky, J., Masojidek, J., van Bergeijk, S., Gabai, S., Shaham, E., Yamshon, A. 2009. Short-term variations in photosynthetic parameters of Nannochloropsis cultures grown in two types of outdoor mass cultivation systems. Aquat. Microb. Ecol. **56**(2-3), 309-322.

[17] Ley, A.C., Mauzerall, D.C. 1982. Absolute absorption cross-sections for Photosystem-II and the minimum quantum requirement for photosynthesis in *Chlorella vulgaris*. Biochim. Biophys. Acta **680**(1), 95-106.

[18] Murakami, R., Hashimoto, H. 2009. Unusual Nuclear Division in Nannochloropsis oculata (Eustigmatophyceae, Heterokonta) which May Ensure Faithful Transmission of Secondary Plastids. Protist **160**(1), 41-49.

[19] Pal, D., Khozin-Goldberg, I., Cohen, Z., Boussiba, S. 2011. The effect of light, salinity and nitrogen availability on lipid production by Nannochloropsis sp. Appl. Microbiol. Biotechnol. 90, 1429–1441.

[20] Ort, D.R., Zhu, X., Melis, A. 2011. Optimizing Antenna Size to Maximize Photosynthetic Efficiency. Plant Physiol. **155**(1), 79-85.

[21] Raven, J.A. 2011. The cost of photoinhibition. Physiol. Plant. **142**(1), 87-104.

[22] Ritchie, R.J. 2008. Universal chlorophyll equations for estimating chlorophylls a, b, c, and d and total chlorophylls in natural assemblages of photosynthetic organisms using acetone, methanol, or ethanol solvents. Photosynthetica **46**(1), 115-126.

[23] Ritchie, R.J., Larkum, A.W.D. 2012. Modelling photosynthesis in shallow algal production ponds. Photosynthetica **50**(4), 481-500.

[24] Rogers, J.N., Rosenberg, J.N., Guzman, B.J., Oh, V.H., Mimbela, L.E., Ghassemi, A., Betenbaugh, M.J., Oyler, G.A., Donohue, M.D. In press. A critical analysis of paddlewheel-driven raceway ponds for algal biofuel production at commercial scales. Algal Res.

[25] Schreiber, U. 2004. Pulse-amplitude-modulation (PAM) fluorometry and saturation pulse method: An overview, in: Papageorgiou, G.C. (Ed.), Chlorophyll a Fluorescence: Signature of Photosynthesis. Springer, pp. 279-319.

[26] Schreiber, U., Klughammer, C., Kolbowski, J. 2012. Assessment of wavelength-dependent parameters of photosynthetic electron transport with a new type of multi-color PAM chlorophyll fluorometer. Photosynt. Res. **113**(1-3), 127-144.

[27] Schreiber, U., Klughammer, C. 2013. Wavelength-dependent photodamage to Chlorella investigated with a new type of multi-color PAM chlorophyll fluorometer. Photosynth. Res. **114**(3), 165-177.

[28] Sforza, E., Simionato, D., Giacometti, G.M., Bertucco, A., Morosinotto, T. 2012. Adjusted Light and Dark Cycles Can Optimize Photosynthetic Efficiency in Algae Growing in Photobioreactors. Plos One **7**(6).

[29] Suggett, D.J., Moore, C.M., Hickman, A.E., Geider, R.J. 2009. Interpretation of fast repetition rate (FRR) fluorescence: signatures of phytoplankton community structure versus physiological state. Mar. Ecol. Prog. Ser. **376**, 1-19.

[30] Sukenik, A., Beardall, J., Kromkamp, J.C., Kopecky, J., Masojidek, J., van Bergeijk, S., Gabai, S., Shaham, E., Yamshon, A. 2009. Photosynthetic performance of outdoor Nannochloropsis mass cultures under a wide range of environmental conditions. Aquat. Microb. Ecol. **56**(2-3), 297-308.

[31] Sukenik, A., Carmeli, Y. and Berner, T. 1989. Regulation of fatty acid composition by irradiance level in the eustigmatophyte Nannochloropsis sp. J. Phycol. 25, 686–692.

[32] Tamburic, B., Guruprasad, S., Radford, D.T., Szabo, M., Lilley, R.M., Larkum, A.W.D., Franklin, J.B., Kramer, D.M., Blackburn, S.I., Raven, J.A., Schliep, M., Ralph, P.J. 2014. The Effect of Diel Temperature and Light Cycles on the Growth of Nannochloropsis oculata in a Photobioreactor Matrix. Plos One **9**(1).

[33] Whittle, S.J., Casselton, P.J. 1975. The chloroplast pigments of the algal classes Eustigmatophyceae and Xanthophyceae. I. Eustigmatophyceae. Br. Phycol. J. **10**, 192-204.

[34] Wondraczek, L., Batentschuk, M., Schmidt, M.A., Borchardt, R., Scheiner, S., Seemann, B., Schweizer, P., Brabec, C.J. 2013. Solar spectral conversion for improving the photosynthetic activity in algae reactors. Nat. Commun. **4**.

[35] Zhang, X.L., Yan, S., Tyagi, R.D., Surampalli, R.Y. 2013. Biodiesel production from heterotrophic microalgae through transesterification and nanotechnology application in the production. Renew. Sustain. Energy Rev. **26**, 216-223.

Figure captions

Fig. 1. $\sigma_{II}(\lambda)$ in dilute suspensions of *N. oculata* (see Section 2.2) grown either at LL (closed symbols, solid line) or HL (open symbols, dashed line) conditions. $\sigma_{II}(\lambda)$ was derived from automated measurements of five consecutive O–I_1 rise curves in the presence of far-red background light. Time between consecutive O–I_1 measurements was 10 s. Values are shown as averages (n=4) ± S.E. (standard errors)

Fig. 2. Effective quantum yield (Y(II)) (a, b) and non-photochemical quenching (NPQ) (c, d) in *N. oculata* grown either at LL (closed symbols, solid line) or HL (open symbols, dashed line) conditions based on steady-state light curve measurements using 440 nm (a, c) and 540 nm (b, d) excitation light. NPQ was calculated as $F_M/F_M`-1$. Values are shown as averages (n=4) ± S.E.

Fig. 3. Effective quantum yield of PSII (Y(II)) (a) and non-photochemical quenching (NPQ) (b) in *N. oculata* grown either at LL (closed symbols, solid line) or HL (open symbols, dashed line) conditions as a function of wavelength at 300 µmol photons.m^{-2}.s^{-1} (circles) and 1200 µmol photons.m^{-2}.s^{-1} (squares). Dark-adapted, maximal quantum efficiency of PSII (termed as $Y(II)_{max}$, triangles) is shown in panel (a). NPQ was calculated as F_M/F_M' -1. Values are shown as averages (n=4) ± S.E.

Fig. 4. Steady-state light curves of rETR using 440 nm (a) and 540 nm (b) irradiance measured with a dilute suspension of *N. oculata* (see Methods) grown either at LL (closed symbols, solid line) or HL (open symbols, dashed line) conditions. Illumination time at each intensity setting was 3 min. Wavelength-dependent parameters of rETR, the maximal electron transport rates ($rETR_{max}$, c) and light intensity at onset of saturation (E_k, d). $rETR_{max}$ and E_k parameters were obtained by fitting the light curves using a PamWin-3 software routine based on the model of (Eilers & Peeters, 1988). Values are shown as averages (n=4) ± S.E.

Fig. 5. Comparison of relative (a, b) and absolute ETR (*ETR*(II)) (c, d) values in LL (a and c) and HL (b and d) at excitations of 440 nm (closed symbols) and 540 nm (open symbols). rETR data was replotted from Fig. 4 a, b. *ETR*(II) curves were derived from rETR by transformation of the PAR-scale into a *PAR*(II) scale according to Schreiber *et al* (2012). The $\sigma_{II}(\lambda)$ values applied for 440 and 540 nm are plotted in Fig. 1. Values are shown as averages (n=4) ± S.E.

Fig. 6. Calculated $ETR(II)_{max}$ values of *N. oculata* grown either at LL (closed symbols, solid line) or HL (open symbols, dashed line) as a function of the wavelength of actinic light (a) and the HL/LL ratios of $ETR(II)_{max}$ (circles) as a function of the wavelength of actinic light (b). Values are shown as averages (n=4) ± S.E.

Footnote. Abbreviations: E_k, light intensity at onset of saturation; *ETR*(II), absolute electron turnover rate of PSII; MC-PAM, multi-colour pulse amplitude modulated chlorophyll fluorometer; NPQ, non-photochemical quenching; *PAR*(II), PSII photon absorption rate; rETR, relative rate of PSII turnover; $rETR_{max}$, maximal relative rate of PSII turnover; $\sigma_{II}(\lambda)$, wavelength-dependent absorption cross-section of PSII; SSLC, steady-state light curve

Percentage of FAME[a]	*N. oculata* HL (300 µmol photons.m^{-2}.s^{-1})	*N. oculata* LL (20 µmol photons.m^{-2}.s^{-1})
	Saturated Fatty acids	
14:0	0.57 ± 0.04	0.30 ± 0.11
16:0	42.63 ± 0.69	39.07 ± 1.41
18:0	3.66 ± 0.24	3.05 ± 0.52
	Unsaturated Fatty acids	
16:1 n-7	20.79 ± 0.78	12.23 ± 0.63
18:1 n-9	18.94 ± 0.35	11.71 ± 0.37
18:2 n-6	1.94 ± 0.04	1.62 ± 0.05
18:3 n-6	0.88 ± 0.05	1.59 ± 0.06
20:4 n-6	1.65 ± 0.02	2.86 ± 0.63
20:5 n-3	8.92 ± 0.12	25.07 ± 0.70
sum SFA[b]	46.86	42.42
sum PUFA[b]	13.39	31.14
	Total FAME content	
g FAME.100 g^{-1} DW	4.49 ± 0.05	4.21 ± 0.09

[a] 15:0, 18:3 n-3, 18:3 n-6, 20:0, 20:2 n-6, 20:3 n-6 and 22:0 were present at less than 0.2% [b] SFA-saturated fatty acids, PUFA – Polyunsaturated fatty acids

Table 1. Proportions (%) of FAMEs of HL and LL *N. oculata* samples. The total FAME amount is expressed as g per 100 g dry weight (DW) (according to Converti et al., 2009).

Figure 1

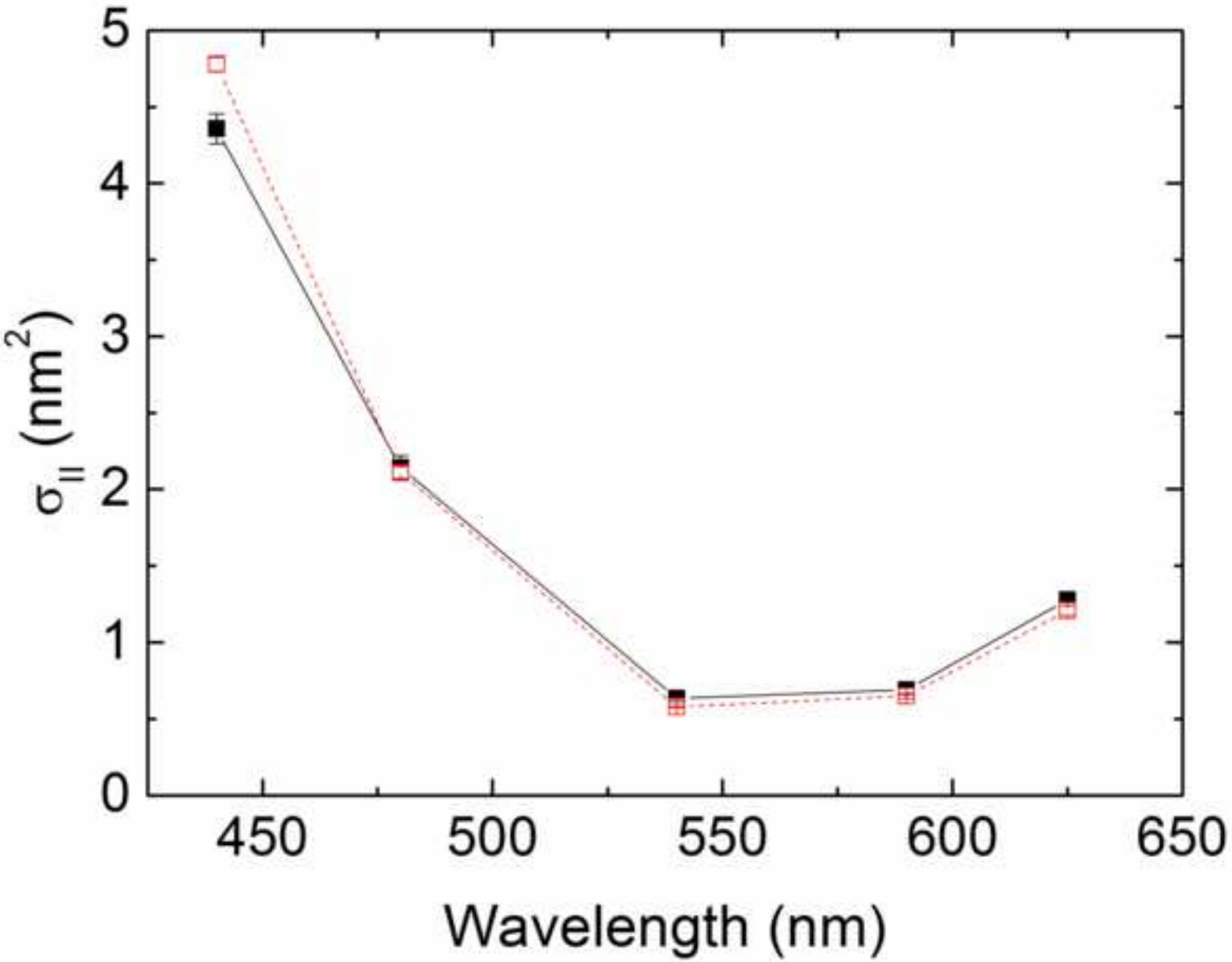

Figure 2

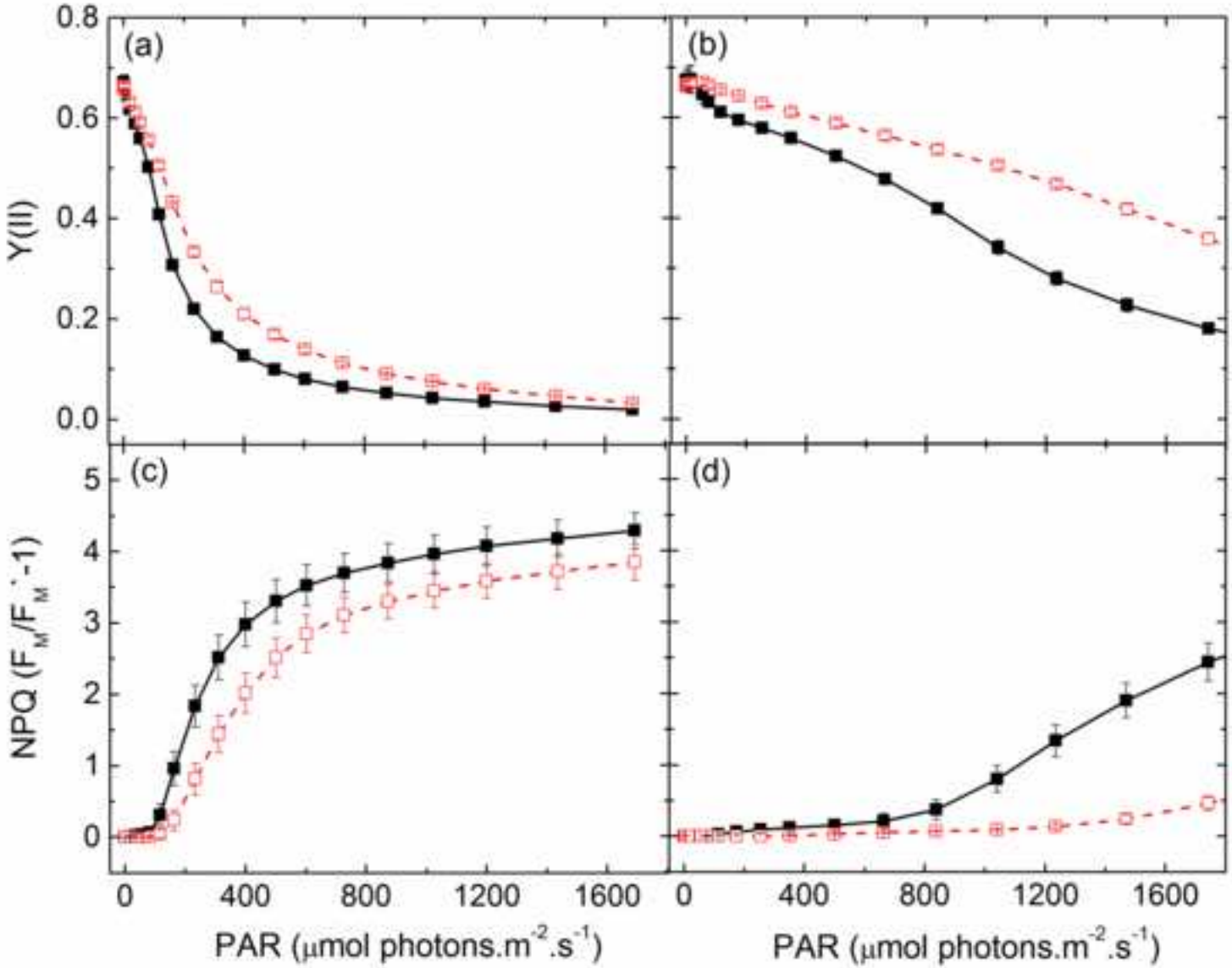

Figure 3

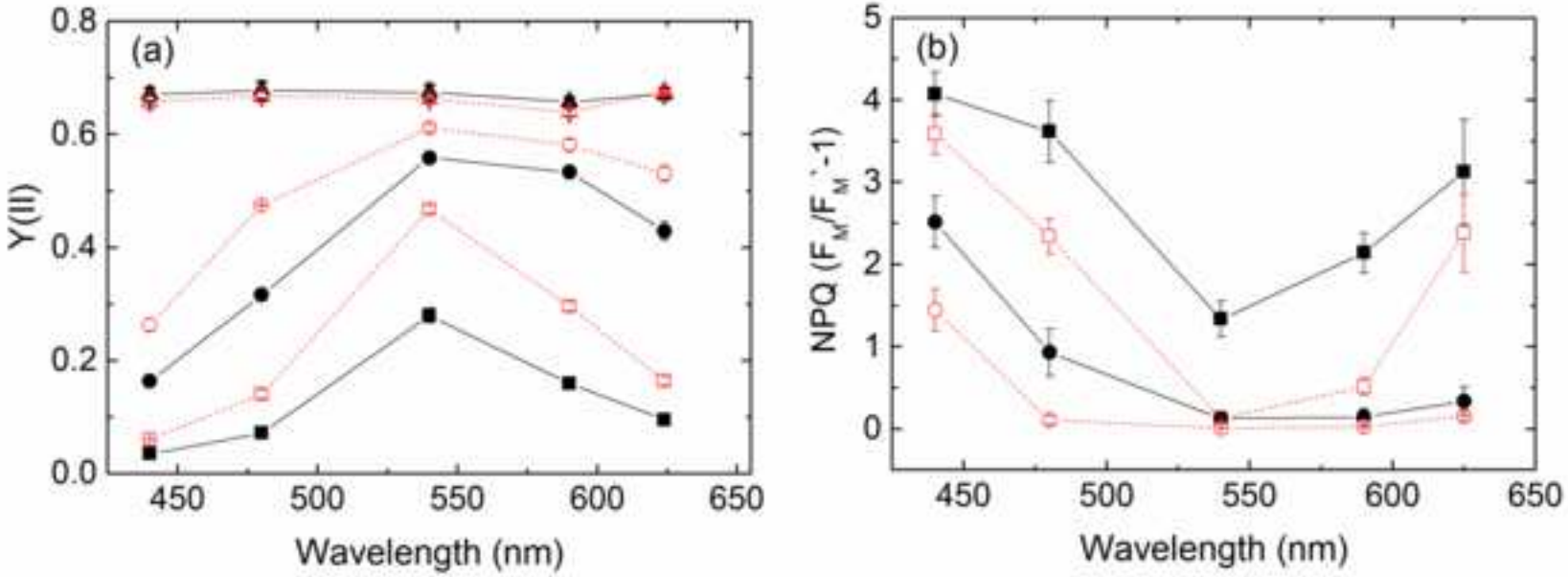

Figure 4

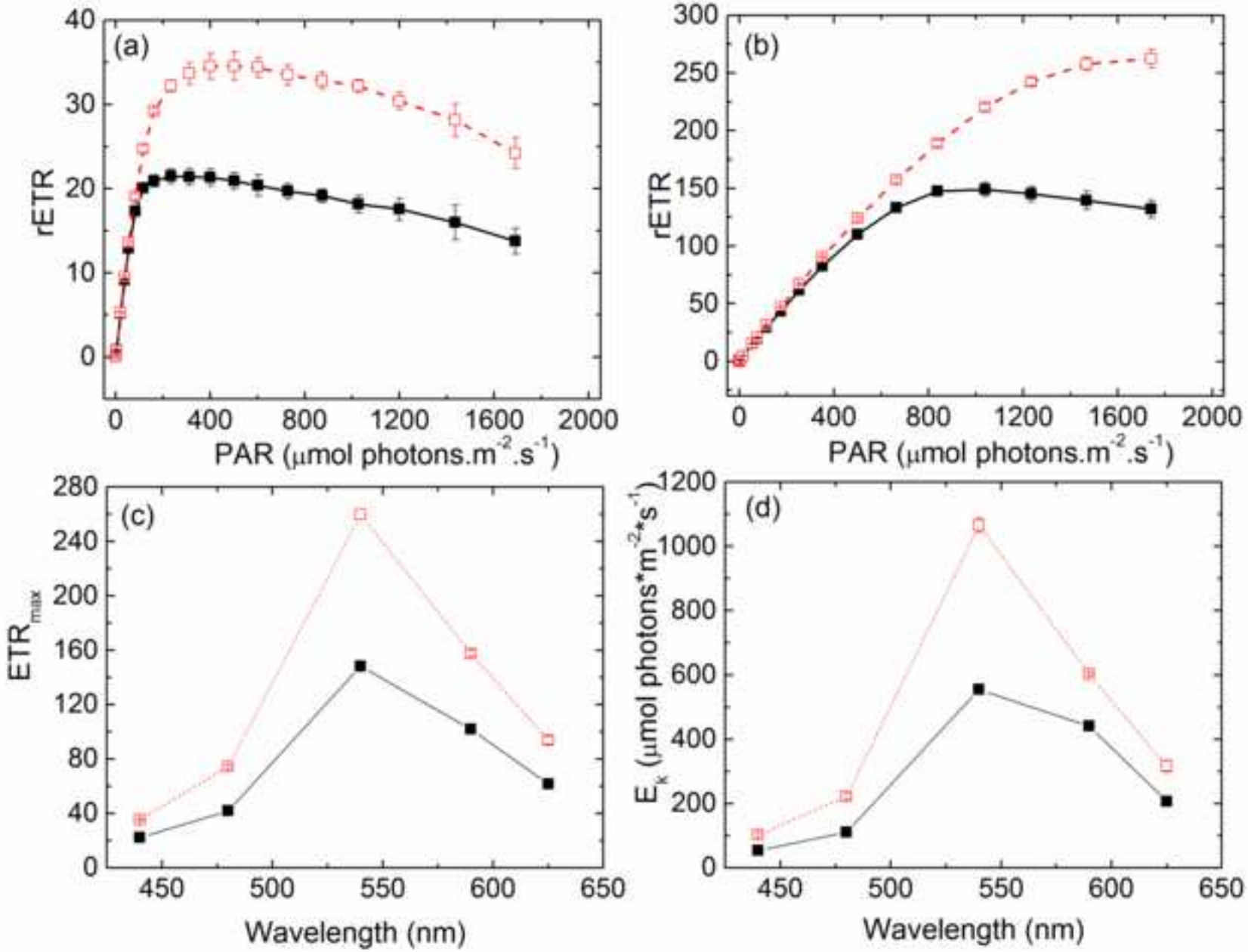

Figure 5

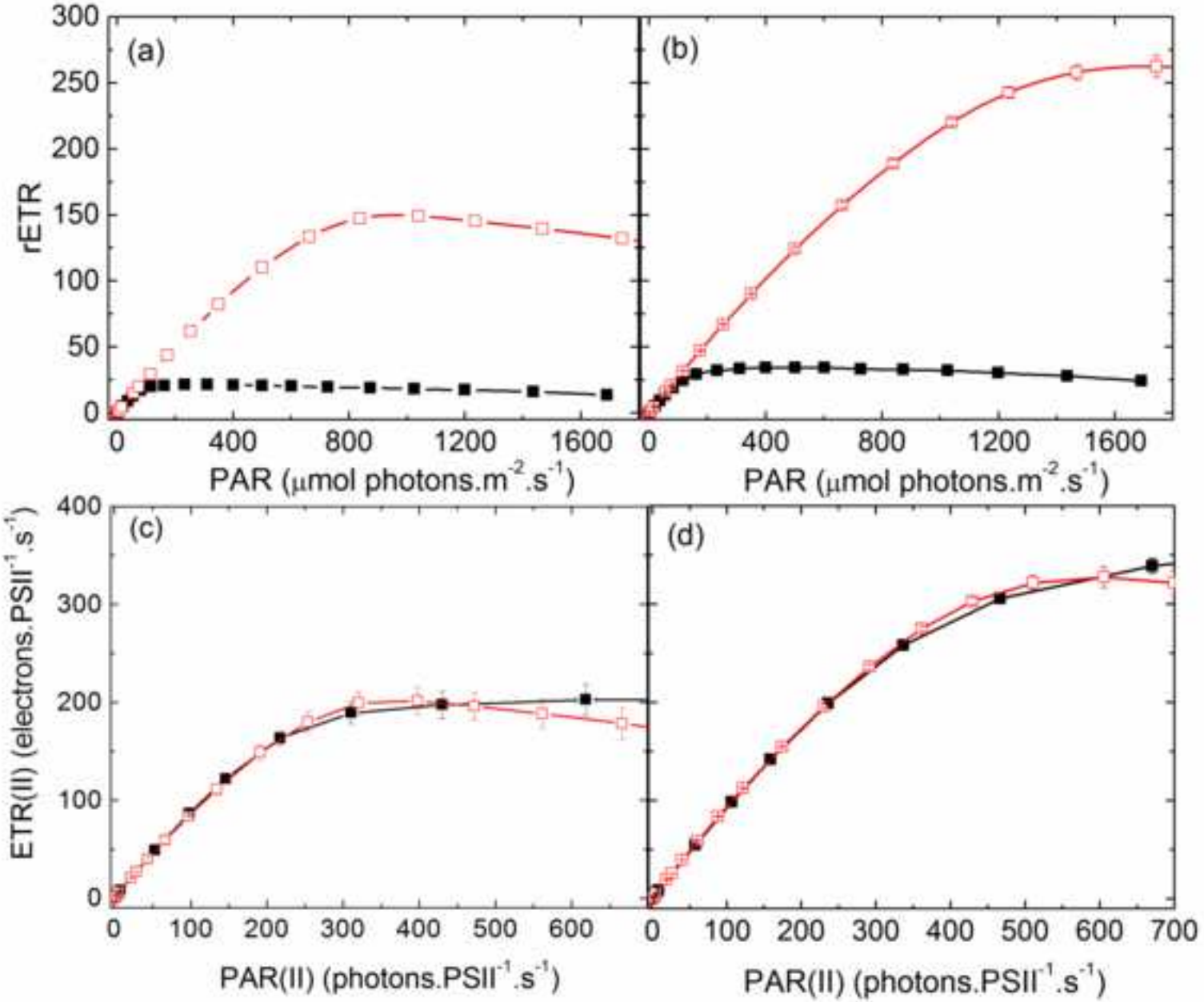

Figure 6

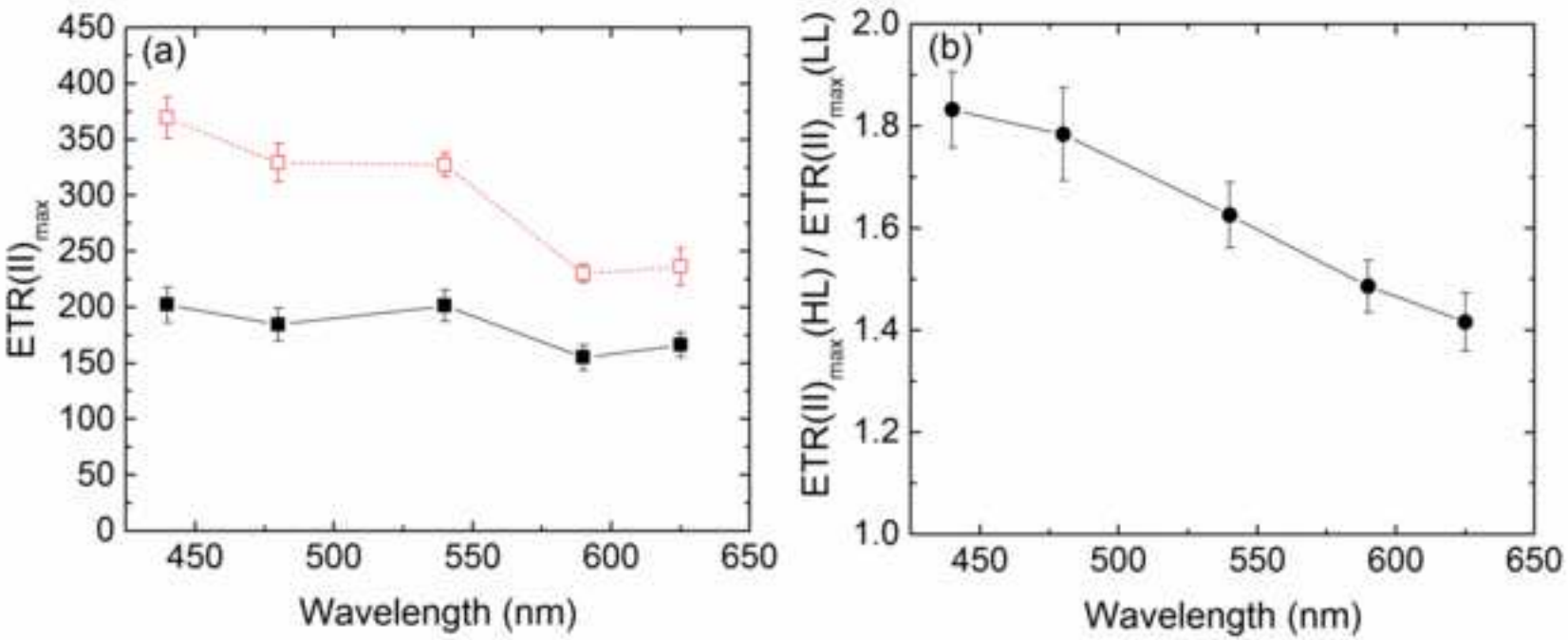

Highlights

1. Multi-wavelength chlorophyll fluorescence on *Nannochloropsis oculata* was analysed.
2. Wavelength-specific light acclimation was found under varying growth irradiances.
3. Elevated absolute electron transfer rates were found under high growth irradiance.
4. Optimal photosynthetic productivity occurs in the blue-green spectral region.
5. Variations in growth irradiance affected the fatty acid composition.